Phase modulation of directed transport, energy diffusion, and quantum scrambling in a Floquet non-Hermitian system

Wen-Lei Zhao [1,*], Guanling Li [1], and Jie Liu [2,3,†]

[1] School of Science, Jiangxi University of Science and Technology, Ganzhou 341000, China
[2] Graduate School of China Academy of Engineering Physics, Beijing 100193, China
[3] CAPT, HEDPS, and IFSA Collaborative Innovation Center of the Ministry of Education, Peking University, Beijing 100871, China

(Received 5 January 2024; accepted 12 August 2024; published 4 September 2024)

We investigate both analytically and numerically the wavepacket's dynamics in momentum space for a Floquet non-Hermitian system with a periodically kicked driven potential. We have deduced the exact expression of a time-evolving wavepacket under the condition of quantum resonance. With this analytical expression, we can investigate thoroughly the temporal behaviors of the directed transport, mean energy, and quantum scrambling. We find interestingly that, by tuning the relative phase between the real part and imaginary part of the kicking potential, one can manipulate the directed transport, mean energy, and quantum scrambling efficiently: When the phase equals to $\pi/2$, we observe a maximum directed transport and mean energy, while a minimum scrambling phenomenon protected by the $\mathcal{PT}$ symmetry; when the phase is π, both the directed transport and the time dependence of the energy are suppressed; in contrast, the quantum scrambling is enhanced by the non-Hermiticity. For the quantum nonresonance case, we numerically find that the quantum interference effects lead to dynamical localization, characterized by the suppression of the directed transport, the time dependence of the energy, and quantum scrambling. Interestingly, these suppression effects can be adjusted by the phase of the non-Hermitian kicking potential. Possible applications of our findings are discussed.

DOI: 10.1103/PhysRevResearch.6.033249

I. INTRODUCTION

Engineering the wavepacket's dynamics, such as directed transport [1–4], energy diffusion [5–9], and information scrambling [10–12], is of great interest both theoretically and experimentally across various fields of physics [13,14]. The phase incorporated in Floquet driven potentials is vitally a knob to manipulate the quantum dynamics [15]. For example, the temporal modulation of the phase of laser standing waves can be used to create artificial gauge fields for ultracold neutral atoms, mimicking the transport behavior of electrons in a synthetic nanotube, with the Aharonov-Bohm flux controllable by the phase [16–18]. The quasiperiodically modulated phase of the external driven potential even induces the formation of synthetic dimension [19–22], wherein the Anderson metal-insulator transition of disorder systems is experimentally observed by using a variant of the kicked rotor model [23–25]. More significantly, complex potentials are achievable in atom-optical experiments, where precise control over the relative phase between the real and imaginary components of this non-Hermitian potential allows for the realization of distinct symmetry classes of systems [26,27].

*Contact author: wlzhao@jxust.edu.cn
†Contact author: jliu@gscaep.ac.cn

Nowadays, non-Hermiticity is widely acknowledged as a fundamental extension of conventional quantum mechanics [28,29] because of its natural incorporation of the gain and loss or nonreciprocity in diverse systems like photonic crystals [30–35], acoustic arrays [36,37], and electrical circuits [38,39]. The emergence of the complex eigenspectra of non-Hermitian systems gives rise to rich phenomena with no Hermitian counterpart. For example, as the system adiabatically crosses the exceptional points at which both the eigenvalues and eigenstates coalesce, the Landau-Zener tunneling emerges, indicating the breakdown of adiabaticity [40–43]. The spontaneous $\mathcal{PT}$-symmetry breaking induces the quantized acceleration of directed transport [44] and the quantized response of quantum scrambling [45] in non-Hermitian chaotic systems [46]. In addition, various topological symmetry classes, including point gap and line gap eigenbands in the complex plane, have been recognized as having significant impacts on edge-state transport behavior, for instance non-Hermitian skin effects [47–50]. Besides, the non-Hermitian potential can be engineered effectively in versatile platforms of photonic systems [51,52] and atom-optics [27], which unveils the possibilities for manipulating the wavepacket's dynamics in a controllable manner.

In this context, we investigate both analytically and numerically the phase modulation of the directed transport, the time dependence of the energy, and quantum scrambling, in a non-Hermitian quantum kicked rotor (NQKR) model with quantum resonance condition. The directed transport of the NQKR model is defined by the time evolution of the expectation of momentum. We find that the relative phase between the real part and imaginary part of the kicking potential dominates the wavepacket's dynamics. Specifically, as time evolves, the directed transport undergoes a crossover from quadratic growth, dependent on the non-Hermitian driving strength, to linear growth, which becomes independent of the non-Hermitian driving strength. Such a dynamical crossover from non-Hermiticity dependent regime to non-Hermiticity independent regime is also observed in the ballistic diffusion of mean energy. Furthermore, we unveil the quadratic growth in the out-of-time ordered correlators (OTOCs) during the initial stages of time evolution and a crossover to linear growth after a sufficiently long period, both influenced by the non-Hermitian driving strength. It is worth noting that the OTOCs we employed coincide with the variance of the energy. Interestingly, when the phase equals to $\pi/2$ ensuring $\mathcal{PT}$ symmetry, we observe a maximum transport behavior and a minimum scrambling phenomenon. At a phase of π, both the directed transport and the time dependence of the energy are suppressed, in contrast the quantum scrambling is enhanced by the non-Hermiticity.

For quantum nonresonance case, we find the dynamical localization [53–55] for the non-Hermitian system, characterized by the saturation behavior of directed transport, mean energy, and OTOCs during time evolution. Interestingly, their saturated values can be effectively adjusted by the phase of non-Hermitian kicking potential. In the semiclassical regime (i.e., $\hbar_{\rm eff} \to 0$), the OTOCs increase exponentially with time, and the growth rate is larger than the classical Lyapunov exponent of the Hermitian kicked rotor model. Our findings provide theoretical guidance for Floquet engineering of quantum dynamics in non-Hermitian systems, which has significant implications in various physics fields, including quantum chaotic control and condensed matter physics.

The paper is organized as follows. In Sec. II, we describe the system. In Sec. III, we show the phase modulation of wavepacket's dynamics with an emphasis on the directed transport, the time-dependence of the energy, and quantum scrambling in quantum resonance case. In Sec. IV, we discuss the wavepacket's dynamics in quantum nonresonance case. A summary is presented in Sec. V.

II. NQKR MODEL

The dimensionless Hamiltonian of the NQKR reads

$$\mathrm{H} = \frac{p^2}{2} + V_K(\theta)\sum_n \delta(t - t_n)\,, \tag{1}$$

with the kicking potential

$$V_K(\theta) = K\cos(\theta) + i\lambda\cos(\theta + \phi), \tag{2}$$

where $p = -i\hbar_{\rm eff}\partial/\partial\theta$ is the angular momentum operator, and θ is the angle coordinate, satisfying the commutation relation $[\theta, p] = i\hbar_{\rm eff}$, with $\hbar_{\rm eff}$ the effective Planck constant. The parameters K and λ represent the strength of the real and imaginary components of the kicking potential, respectively. The relative phase between these two components is determined by the parameter ϕ. This kind of complex potential has been realized in the atom-optics experiment [27].

In the atom-optics experiment, the complex potential in Eq. (2) has been realized by the superposition of two standing laser fields, interacting with ultracold atoms that encompass

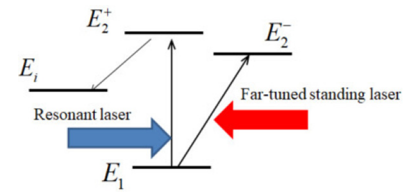

FIG. 1. Schematic of the experiment for the realization complex driven potential. The far-tuned standing laser coupling E_1 and E_2^- generates a dipole force on the atoms, representing the real part of the complex potential. Meanwhile, the resonant laser facilitates the transition from E_1 to E_2^+. The ultracold atoms in E_2^+ then transition to E_i, leading to particle loss and mimicking the imaginary part of the complex potential.

a ground state E_1, excited states with two hyperfine levels $E_2^{\pm}$, and a noninteracting state E_i (see Fig. 1) [26,27]. The far-tuned standing laser, coupling E_1 and E_2^-, generates a dipole force on the atoms, emulating the real component of the complex potential. The resonant laser facilitates the transition from E_1 to E_2^+. The ultracold atoms in E_2^+ subsequently transition to E_i, resulting in particle loss and thereby mimicking the imaginary part of the complex potential. The precise modulation of the relative phase between the real and imaginary parts of the complex potential is achievable by adjusting the distance between the atomic beam and the mirror surface. The delta-kicking potential is emulated using a sequence of short square pulses created through the modulation of the standing wave by an acousto-optical modulator [24].

The eigenequation of angular momentum operator is $p|\varphi_n\rangle = p_n|\varphi_n\rangle$ with eigenvalue $p_n = n\hbar_{\rm eff}$ and eigenstate $\langle\theta|\varphi_n\rangle = e^{in\theta}/\sqrt{2\pi}$. With the completed basis of $|\varphi_n\rangle$, an arbitrary state can be expanded as $|\psi\rangle = \sum_n \psi_n|\varphi_n\rangle$. One-period evolution of the quantum state from t_n to t_{n+1} is governed by $|\psi(t_{n+1})\rangle = U|\psi(t_n)\rangle$, where the Floquet operator $U = U_f U_K$ (or $U = U_K U_f$) is composed of the free evolution $U_f = \exp(-ip^2/2\hbar_{\rm eff})$ and the kicking evolution $U_K = \exp[-iV_K(\theta)/\hbar_{\rm eff}]$.

III. QUANTUM RESONANCE CASE

In the quantum resonance condition (i.e., $\hbar_{\rm eff} = 4\pi$), $U_f(p_n) = \exp(-in^2 2\pi) = 1$, indicating that the U_f is unity. Therefore, the two expressions of the Floquet operator $U = U_f U_K$ and $U = U_K U_f$ are equivalent. One can get the exact express of the quantum state after arbitrary kick period, i.e., $|\psi(t)\rangle = U_K^t|\psi(t_0)\rangle = \exp[-itV_K(\theta)/\hbar_{\rm eff}]|\psi(t_0)\rangle$. In addition, the quantum resonance condition is of particular interest in that the generalized models of the kicked rotor based on this fine tuned point exhibit controllable quantum walk [56], topologically protected transport [57,58] and quantum Hall effect [59].

Without loss of generality, we choose the ground state of the angular momentum operator as the initial state, i.e., $\psi(\theta, t_0) = 1/\sqrt{2\pi}$. Then, the quantum state $|\psi(t)\rangle$ in coordinate space has the expression

$$\psi(\theta, t) = \frac{1}{\sqrt{2\pi}}\exp\left\{\frac{-it}{4\pi}[K\cos(\theta) + i\lambda\cos(\theta + \phi)]\right\}, \tag{3}$$

whose norm takes the form

$$\mathcal{N}(t) = \int_{-\pi}^{\pi} |\psi(\theta,t)|^2 d\theta = I_0\left(\frac{\lambda t}{2\pi}\right). \tag{4}$$

Here, $I_0(x)$ denotes the modified Bessel function of the first kind with zeroth order (See Appendix). The nonunitary evolution is characterized by the unbounded growth of the $\mathcal{N}(t)$ with time, i.e., $\mathcal{N}(t) \approx \exp(\lambda t/2\pi)\sqrt{2\pi/\lambda t}$ for $\lambda t/2\pi \gg 1$.

In the present paper, we investigate both analytically and numerically the dynamics of the momentum current $\langle p(t)\rangle$, mean energy $\langle p^2(t)\rangle$, and quantum scrambling $C(t) = -\langle [A(t), B]^2\rangle$ [60–62]. Note that the $C(t)$ is defined in the Heisenberg picture, with $A(t) = U^\dagger(t)AU(t)$ and $\langle\cdot\rangle = \langle\psi(t_0)|\cdot|\psi(t_0)\rangle$ indicates the expectation value of the operator with respect to the initial state [63,64]. To reduce the impact of the norm to observables, we introduce the rescaled quantities as $\langle p(t)\rangle = \sum_n p_n|\psi_n|^2/\mathcal{N}(t)$ and $\langle p^2(t)\rangle = \sum_n p_n^2|\psi_n|^2/\mathcal{N}(t)$ [65].

We use the operators $A = e^{-i\varepsilon p}$ and $B = |\psi(t_0)\rangle\langle\psi(t_0)|$ to construct OTOCs. Straightforward derivation yields the relation $C(t) = \mathcal{N}^2(t) - |\langle\psi(t)|e^{-i\varepsilon p}|\psi(t)\rangle|^2$ [66]. Then, a natural definition of the rescaled OTOCs is given by $C(t) = 1 - |\langle\psi(t)|e^{-i\varepsilon p}|\psi(t)\rangle|^2/\mathcal{N}^2(t)$ [66]. We consider the case $\varepsilon \ll 1$. Our main results are described by the three following relations:

$$\langle p(t)\rangle = -K\sin(\phi)\frac{I_1\left(\frac{\lambda t}{2\pi}\right)}{I_0\left(\frac{\lambda t}{2\pi}\right)}t, \tag{5}$$

$$\langle p^2(t)\rangle = K^2\sin^2(\phi)t^2 + \frac{2\pi}{\lambda}\frac{I_1\left(\frac{\lambda t}{2\pi}\right)}{I_0\left(\frac{\lambda t}{2\pi}\right)}[K^2\cos(2\phi)+\lambda^2]t, \tag{6}$$

and

$$C(t) \approx K^2\varepsilon^2\sin^2(\phi)t^2\left\{1 - \left[\frac{I_1\left(\frac{\lambda t}{2\pi}\right)}{I_0\left(\frac{\lambda t}{2\pi}\right)}\right]^2\right\} + \frac{2\pi\varepsilon^2 t}{\lambda}\frac{I_1\left(\frac{\lambda t}{2\pi}\right)}{I_0\left(\frac{\lambda t}{2\pi}\right)}[K^2\cos(2\phi)+\lambda^2], \tag{7}$$

where $I_1(x)$ denotes the modified Bessel function of the first kind with order one (see Appendix).

A. Directed transport

Figure 2(a) shows that, for short time, the $\langle p\rangle$ increases in the quadratic function of time with the coefficient depending on λ. Nevertheless, the $\langle p\rangle$ turns to grow with time linearly in a long term evolution with the coefficient not depending on λ. Such a crossover occurs around a critical time t_c. In addition, one can see perfect agreement between numerical results and analytical prediction in Eq. (5). For $\lambda t/2\pi \ll 1$, we have the approximations $I_0(\lambda t/2\pi) \approx 1$ and $I_1(\lambda t/2\pi) \approx \lambda t/4\pi$ (see Appendix). Taking these relations to Eq. (5) yields the relation $\langle p(t)\rangle \approx -K\lambda\sin(\phi)t^2/4\pi$. Apparently, the growth rate $\langle p(t)\rangle/t^2 = -K\lambda\sin(\phi)/4\pi$ increases with the increase of λ, which is validated by our numerical results. For $\lambda t/2\pi \gg 1$, substituting the approximations of both $I_0(\lambda t/2\pi) \approx \exp(\lambda t/2\pi)(1+\pi/4\lambda t)/\sqrt{\lambda t}$ and $I_1(\lambda t/2\pi) \approx \exp(\lambda t/2\pi)(1-3\pi/4\lambda t)/\sqrt{\lambda t}$ (See Appendix) into Eq. (5) results in the linear growth $\langle p(t)\rangle \approx -K\sin(\phi)(t-\pi/|\lambda|)$ with time, for which the coefficient, i.e., $-K\sin(\phi)$ is independent on λ. The above estimations uncover the mechanism for the crossover from quadratic-law growth to the linear growth as time evolves. In addition, our findings of the sinusoidal relationship between mean momentum and phase ϕ pave the way for Floquet engineering of the directed transport in non-Hermitian chaotic systems.

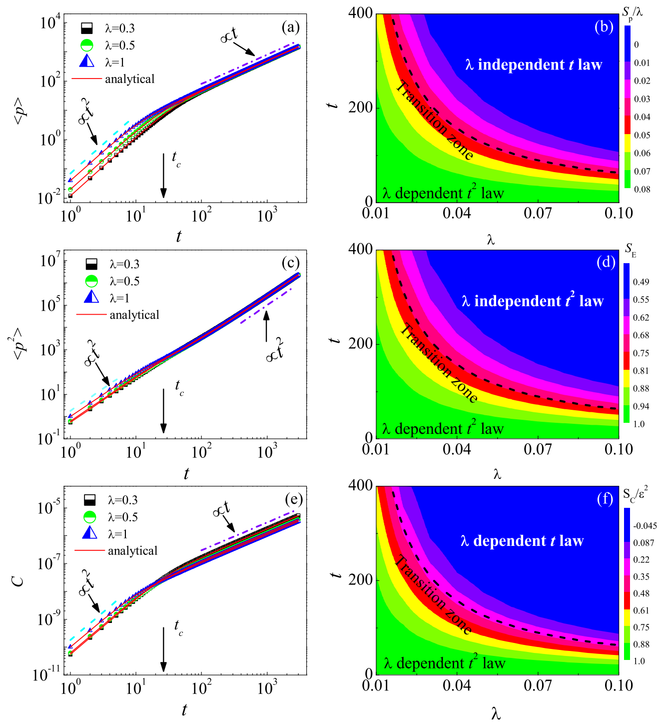

FIG. 2. Left panels: Time dependence of the $\langle p\rangle$ (a), $\langle p^2\rangle$ (c), and C (e) for $\lambda = 0.3$ (squares), 0.5 (circles), and 1 (triangles). Red solid lines in (a), (c), and (e) indicate our analytical predictions in Eqs. (5), (6), and (7), respectively. Arrows mark the threshold value of t_c. Geen-dashed lines denote a square function of time. Violet dash-dotted lines in (a) and (e) denote the linear function of time, while in (b) it indicates the square function of time. Right panels: The values of S_p/λ (b), S_E (d), and S_C/ε^2 (f) in the parameter space (t, λ), which show three distinct zones. Dashed lines denote $t_c = 2\pi/\lambda$. In (e) and (f), the translation parameter is $\varepsilon = 10^{-5}$. The parameters are $K = 1$ and $\phi = -\pi/6$.

To see the change of $\langle p(t)\rangle$'s evolution between short and long time behavior, we investigate the second derivative of the mean momentum $S_p = d^2\langle p(t)\rangle/dt^2$. Note that, in the following derivation, for brevity, we use I_j to replace $I_j(\frac{\lambda t}{2\pi})$ $(j = 0, 1, 2...)$. The analytical expression takes the form

$$S_p = -K\sin(\phi)\frac{\lambda}{2\pi}\left[1 + \frac{I_2}{I_0} - 2\left(\frac{I_1}{I_0}\right)^2\right] + K\sin(\phi)\frac{\lambda^2 t}{4\pi^2}\left[\frac{3I_1 - I_3}{4I_0} + \frac{3I_1I_2}{2I_0^2} - 2\left(\frac{I_1}{I_0}\right)^3\right]. \tag{8}$$

Taking into account the approximation of I_j $(j = 0, 1, 2, 3)$ under two different conditions, namely, when $\lambda t/2\pi \ll 1$ and when $\lambda t/2\pi \gg 1$ (see Appendix), we can derive approximate

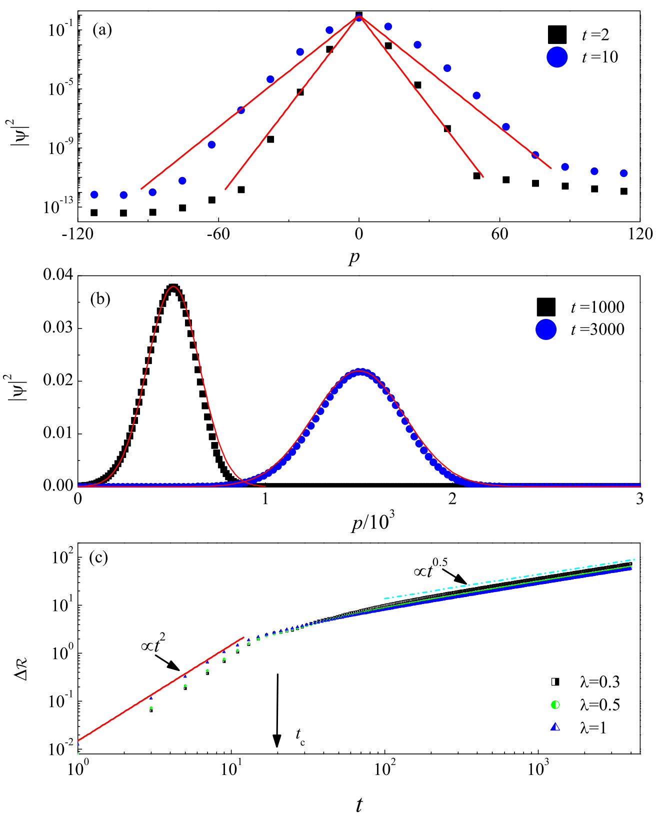

FIG. 3. Momentum distributions for short (a) and long (b) time evolution with $\lambda = 0.3$. In (a), red-solid lines indicate the exponential fitting $|\psi(p)|^2 \sim \exp(-|p|/\xi)$ with $\xi = 2.1$ and 3.43 for $t = 2$ and 10 respectively. In (b), red-solid lines indicate the Gaussian function fitting $|\psi(p)|^2 \sim \exp[-(p-p_c)^2/\sigma]$ with $(p_c = 500, \sigma = 3.9 \times 10^4)$ and $(p_c = 1500, \sigma = 1.2 \times 10^5)$ for $t = 1000$ and 3000 respectively. (c): Time dependence of the inverse participation ratio $\Delta\mathcal{R}(t) = \mathcal{R}(t) - \mathcal{R}(t_0)$ for $\lambda = 0.3$ (squares), 0.5 (circles), and 1 (triangles). Here, $\mathcal{R}(t_0)$ denotes the initial value of the inverse participation ratio. Red-solid line and cyan dash-dotted lines indicate the power law growth, i.e., $\mathcal{R} \propto t^\alpha$ with $\alpha = 2$ and 0.5, respectively. Arrow marks the critical time t_c. Other parameters are same as in Fig. 2(a).

expressions

$$S_p \approx \begin{cases} \frac{-K\sin(\phi)\lambda}{2\pi}, & \text{for } \frac{\lambda t}{2\pi} \ll 1, \\ 0, & \text{for } \frac{\lambda t}{2\pi} \gg 1, \end{cases} \tag{9}$$

In Fig. 2(b), we have plotted the ratio S_p/λ for various values of t and λ. Three distinct zones can be observed: (i) a λ-dependent t^2-law zone with $S_p/\lambda = -K\sin(\phi)/2\pi$ for $t \ll t_c = 2\pi/\lambda$; (ii) a λ-independent t-law zone with $S_p = 0$ for $t \gg t_c$; and (iii) a crossover zone for $t \sim t_c$.

In the λ-dependent t^2-law zone, the quantum state is exponentially localized in momentum space, i.e., $|\psi(p)|^2 \sim \exp(-|p|/\xi)$, whose localization length ξ increases with time [see Fig. 3(a)]. Detailed observations reveal that this exponentially localized shape of the quantum state is asymmetric around $p = 0$. This kind of asymmetric spreading of the quantum state in momentum space results in the growth of mean momentum with time. While in the λ-independent t-law zone, the momentum distribution can be well described by the Gaussian function $|\psi(p)|^2 \sim \exp[-(p-p_c)^2/\sigma]$ [see Fig. 3(b)]. Interestingly, the comparison of the momentum distribution in different time demonstrates that the center momentum p_c linearly increases with time, i.e., $p_c(t) = Dt$ for which the growth rate equal to that of the $\langle p(t)\rangle$, i.e., $D = d\langle p(t)\rangle/dt$. Therefore, the linear growth of the mean momentum for $t \gg t_c$ originates from the directed movement of the soliton-like wavepacket in momentum space. In addition, we would like to stress that the width σ of the Gaussian wavepacket also increases with time.

We numerically investigate the inverse participation ratio (IPR) $\mathcal{R} = (\sum_n |\psi_n|^2)^2/\sum_n |\psi_n|^4$ to measure the localization property of quantum states [67–69]. Our results show that for a specific value of λ [e.g., $\lambda = 0.3$ in Fig. 3(c)], $\mathcal{R}$ increases according to a power law of time, $\mathcal{R} \propto t^\alpha$, with the exponent being 2 for $t \ll t_c$ and 0.5 for $t \gg t_c$. Note that, for exponentially localized wave functions, i.e., $|\psi(p)|^2 \sim \exp(-|p|/\xi)$, the $\mathcal{R}$ is proportional to the localization length ξ. Therefore, our results demonstrate that the localization length ξ increases quadratically with time for $t \ll t_c$. On the other hand, for Gaussian function wavepacket, i.e., $|\psi(p)|^2 \sim \exp[-(p-p_c)^2/\sigma]$, straightforward derivation yields the relation $\mathcal{R} \propto \sqrt{\sigma}$. In our model, the quantum states can be well described by the Gaussian wavepacket after a long-term evolution, for which the variance is proportional to the C. The linear increase of C for $t \gg t_c$ [see Fig. 2(c)] results in the square-root law of the form $\mathcal{R} \propto \sqrt{t}$. Our numerical simulations indicate that the behavior near t_c is a crossover corresponding to a continuous change of the power exponents from 2 to 0.5.

B. Time dependence of the energy

Figure 2(c) illustrates that the energy of the NQKR model diffuses in a ballistic way, i.e., $\langle p^2(t)\rangle = Gt^2$, which is in perfect agreement with our analytical prediction in Eq. (6). Interestingly, for $t \ll t_c$, the diffusion rate G increases with the non-Hermitian parameter λ, and for $t \gg t_c$, it becomes independent of λ. By approximating both $I_0(\lambda t/2\pi)$ and $I_1(\lambda t/2\pi)$ under two different limits, we can derive the approximate expression for Eq. (6), namely, $\langle p^2(t)\rangle \approx (K^2+\lambda^2)t^2/2$ for $t \ll t_c$ and $\langle p^2(t)\rangle \approx K^2\sin^2(\phi)t^2 + 2\pi t[K^2\cos(2\phi) + \lambda^2]/|\lambda|$ for $t \gg t_c$. This confirms the crossover from λ-dependent behavior to λ-independent behavior. This crossover can also be observed in the second derivative of the mean square of momentum, denoted as $S_E = d^2\langle p^2(t)\rangle/dt^2$,

$$S_E = 2K^2\sin^2(\phi) - \frac{2\pi S_p}{K\lambda\sin(\phi)}[K^2\cos(2\phi) + \lambda^2], \tag{10}$$

which can be approximated as

$$S_E \approx \begin{cases} K^2 + \lambda^2, & \text{for } \frac{\lambda t}{2\pi} \ll 1, \\ 2K^2\sin^2(\phi), & \text{for } \frac{\lambda t}{2\pi} \gg 1. \end{cases} \tag{11}$$

In Figure 2(d), we present numerical results of S_E based on Eq. (10), which demonstrates the λ-dependent zone for $t \ll t_c$, a crossover zone for $t \sim t_c$, and the λ-independent zone for $t \gg t_c$. Our discovery of the sinusoidal dependence of S_E on phase ϕ provides a theoretical foundation for engineering the time dependence of the energy through non-Hermitian driven potential.

C. Quantum scrambling

Based on the Taylor expansion $e^{-i\varepsilon p} \approx 1 - i\varepsilon p$ for $\varepsilon \ll 1$, we obtain the relations

$$\begin{aligned} C(t) &\approx \varepsilon^2[\langle p^2\rangle - \langle p\rangle^2] \\ &= K^2\varepsilon^2 \sin^2(\phi)t^2\left[1 - \left(\frac{I_1}{I_0}\right)^2\right] \\ &\quad + \frac{2\pi\varepsilon^2 t}{\lambda}\frac{I_1}{I_0}[K^2\cos(2\phi) + \lambda^2], \end{aligned} \tag{12}$$

which has two different asymptotic behaviors

$$C(t) \approx \begin{cases} \frac{\varepsilon^2(K^2+\lambda^2)}{2}t^2, & \text{for } \lambda t/2\pi \ll 1, \\ \frac{2\pi\varepsilon^2}{|\lambda|}\left[\frac{1+\cos(2\phi)}{2}K^2 + \lambda^2\right]t, & \text{for } \lambda t/2\pi \gg 1. \end{cases} \tag{13}$$

In Fig. 2(e), we show our numerical results for the time evolution of C for different λ. It is evident that C exhibits a quadratic growth with time for $t \ll t_c$ and a linear growth with time for $t \gg t_c$, with both behaviors being dependent on λ. These distinct behaviors are also characterized by the second derivative $S_C = d^2C(t)/dt^2$. Straightforward derivation yields the relation

$$S_C = \varepsilon^2\left[S_E - 2\left(\frac{d\langle p\rangle}{dt}\right)^2 - 2\langle p\rangle S_p\right], \tag{14}$$

with

$$\frac{d\langle p\rangle}{dt} = -K\sin(\phi)\left\{\frac{\lambda t}{4\pi}\left[1 + \frac{I_2}{I_0} - 2\left(\frac{I_1}{I_0}\right)^2\right] + \frac{I_1}{I_0}\right\}. \tag{15}$$

By approximating the terms on the right side of Eq. (14) under two different limits, we derive the approximate relation

$$S_C \approx \begin{cases} \varepsilon^2(K^2+\lambda^2), & \text{for } \lambda t/2\pi \ll 1, \\ 0, & \text{for } \lambda t/2\pi \gg 1. \end{cases} \tag{16}$$

Our numerical results, based on Eq. (14), clearly demonstrate the λ-dependent quadratic growth zone for $t \ll t_c$, the crossover zone for $t \sim t_c$, and the λ-dependent linear growth zone for $t \gg t_c$ [see Fig. 2(f)], validating our analytical prediction in Eq. (16).

D. Some remarks on the relation between phase manipulation and $\mathcal{PT}$ symmetry

The dependence of the long-time behavior of the $\langle p\rangle$, $\langle p^2\rangle$, and C on the phase ϕ opens the opportunity for the manipulation of both the quantum transport and quantum scrambling via the relative phase between the real part and the imaginary part of the kicking potential $V_K(\theta) = K\cos(\theta) + i\lambda\cos(\theta + \phi)$ [see Eq. (2)]. Interestingly, the potential is $\mathcal{PT}$ symmetric when $\phi = \pi/2$ [70]. In this situation, both directed transport and mean energy reach their maximum values, namely, $\langle p\rangle \approx -Kt$ and $\langle p^2\rangle \approx K^2t^2$ since $\langle p\rangle$ and $\langle p^2\rangle$ are sinusoidal functions of ϕ, signaling the $\mathcal{PT}$-symmetry protected transport behaviors. In contrast, quantum scrambling is minimized,

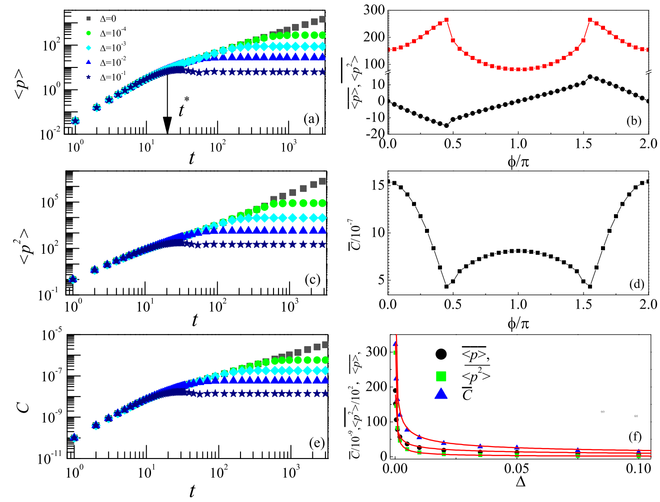

FIG. 4. Time dependence of $\langle p\rangle$ (a), $\langle p^2\rangle$ (c), and C (e) with $\lambda = 1$ for $\hbar_{\text{eff}} = 4\pi + \Delta$ with $\Delta = 0$ (squares), 10^{-4} (circles), 10^{-3} (diamonds), 10^{-2} (triangles), and 10^{-1} (pentagrams). Arrow in (a) marks the critical time t^*. (b) The $\overline{\langle p\rangle}$ (circles) and $\overline{\langle p^2\rangle}$ (squares) vs ϕ for $\Delta = 0.1$. (d) The $\overline{C}$ (triangles) vs ϕ for $\Delta = 0.1$. (f) The $\overline{\langle p\rangle}$ (circles), $\overline{\langle p^2\rangle}$ (squares), and $\overline{C}$ (triangles) vs Δ for $\phi = -\pi/6$. Red-solid lines indicate power-law fittings $\propto t^{-\beta}$, with the exponent β being 0.44 for $\overline{\langle p\rangle}$, 0.8 for $\overline{\langle p^2\rangle}$, and 0.5 for $\overline{C}$. Other parameters are same as in Fig. 2(a).

i.e., $C \approx 2\pi\varepsilon^2|\lambda|t$ because C behaves as a cosine function of 2ϕ (see Table I). For $\phi = \pi$, the NQKR model is a general non-Hermitian system that does not have $\mathcal{PT}$ symmetry, for which the directed transport is totally suppressed, namely, $\langle p\rangle = 0$, and the mean energy reduces as $\langle p^2\rangle \propto t$. In contrast the C is maximum $C \approx 2\pi\varepsilon^2 t(K^2 + \lambda^2)/|\lambda|$ demonstrating the non-Hermiticity enhanced quantum scrambling.

IV. QUANTUM NONRESONANCE CASE

It is well known that in the Hermitian kicked rotor model, some interesting things, such as ergodicity breaking and dynamical localization, occur in the quantum nonresonance regime [71]. Therefore, we further investigate the dynamics of momentum current, mean energy, and quantum scrambling away from the quantum resonance regime, i.e., $\hbar_{\text{eff}} = 4\pi + \Delta$. For a very small Δ [e.g., $\Delta = 10^{-4}$ in Fig. 4(a)], the $\langle p\rangle$ follows that of $\Delta = 0$ during finite-time evolution, i.e., $t < t^*$, and gradually saturates when $t > t^*$. Moreover, both the critical time t^* and the saturation level decrease with the increase of Δ. It is reasonable to believe that the quantum interference effects, which lead to dynamical localization, suppress the directed transport in momentum space. The appearance of dynamical localization of mean energy is shown clearly in Fig. 4(c), where one can see that saturation level of $\langle p^2\rangle$ decreases with the increase of Δ. After a long-term evolution, the OTOCs for a nonzero value of Δ [e.g., $\Delta = 10^{-4}$ in Fig. 4(e)] exhibit saturation behavior as well. The saturated value decreases as Δ increases, indicating the freezing of quantum scrambling due to dynamical localization.

We numerically investigate the saturation values of the momentum current, mean energy, and quantum scrambling,

TABLE I. Symmetry and the long-time behavior of the $\langle p\rangle$, $\langle p^2\rangle$, and C for $\phi = -\pi/2$ and π.

Phase ϕ	$-\pi/2$	π
Symmetry class	$\mathcal{PT}$	non-$\mathcal{PT}$
Directed transport $\langle p(t)\rangle \propto -K\sin(\phi)t$	$\propto Kt$	0
Mean energy $\langle p^2(t)\rangle \propto K^2\sin^2(\phi)t^2 + 2\pi[K^2\cos(2\phi)+\lambda^2]t/\lvert\lambda\rvert$	$\propto K^2t^2$	$\propto \frac{2\pi}{\lvert\lambda\rvert}(K^2+\lambda^2)t$
Quantum scrambling $C(t) \propto \frac{2\pi\varepsilon^2}{\lvert\lambda\rvert}\left[\frac{1+\cos(2\phi)}{2}K^2+\lambda^2\right]t$	$\propto 2\pi\varepsilon^2\lambda t$	$\propto \frac{2\pi\varepsilon^2}{\lvert\lambda\rvert}(K^2+\lambda^2)t$

denoted by $\overline{\langle p\rangle}$, $\overline{\langle p^2\rangle}$, and $\overline{C}$, respectively, for different ϕ [72]. Our results show that $\overline{\langle p\rangle}$ exhibits three different behaviors: (i) a linear decrease for ϕ smaller than $\approx \pi/2$; (ii) a linear increase for ϕ larger than $\approx \pi/2$ and smaller than $\approx 3\pi/2$; and (iii) a linear decrease for $\phi > 3\pi/2$ [see Fig. 4(b)]. The crossover between these different regimes are sharp, indicating the occurrence of discontinuities tuned by the non-Hermitian kicking potential. Interestingly, $\overline{\langle p^2\rangle}$ also exhibits three distinct regimes. With the increase of ϕ, it increases monotonically for $\phi < \pi/2$, decreases continuously to reach a minimum at $\phi = \pi$, then increases again for $\phi < 3\pi/2$, and finally decreases for $\phi > 3\pi/2$. The trend of $\overline{C}$ with respect to ϕ shows an opposite behavior compared to $\overline{\langle p^2\rangle}$, suggesting the emergence of discontinuities controlled by ϕ as well [see Fig. 4(d)]. We further numerically investigate the asymptotic values, i.e., $\overline{\langle p\rangle}$, $\overline{\langle p^2\rangle}$, and $\overline{C}$, for $\Delta \to 0$. For a specific ϕ [e.g., $\phi = -\pi/6$ in Fig. 4(f)], they all exhibit a power-law divergence, i.e., $\propto t^{-\beta}$ as $\Delta \to 0$.

An interesting issue of quantum chaos is the comparison of quantum behavior with its classical limit ($\hbar_{\text{eff}} \to 0$). For any finite $\hbar_{\text{eff}}$, the Hermitian kicked rotor model follows the classical chaos behavior up to a finite time, i.e., Ehrenfest time t_E, beyond which quantum integrable behavior appears and the system stops absorbing energy. It has been found that, in the Hermitian kicked rotor model, the dynamics of OTOCs $C_Q = -\langle [p(t), p]^2\rangle$ is in good agreement with its classical counterpart $C_{cl} \approx \hbar_{\text{eff}}^2 \langle\langle (\Delta p(t)/\Delta\theta(0))^2\rangle\rangle_{cl} \propto e^{2\gamma t}$ within the Ehrenfest time, i.e., $t < t_E$ [73]. Here, the $\langle\langle \cdots \rangle\rangle_{cl}$ denotes the average of the differences of two neighboring trajectories over the classical phase space. For $t > t_E$, the ergodicity breaking destroys the classically chaotic behavior of OTOCs and results in a quadratic increase [73,74]. We further investigate the OTOCs for very small $\hbar_{\text{eff}}$ to see if quantum effects affect chaos also in non-Hermitian case. It is worth noting that the classical limit of non-Hermitian systems is still an elusive issue [75,76]. Therefore, we only compare quantum OTOCs in our non-Hermitian model with the classical OTOCs in the standard Hermitian kicked rotor model.

Our investigation shows that, for very small λ [e.g., $\lambda = 0.00008$ in Fig. 5(a)], the OTOCs follow the classically chaotic behavior, i.e., $C_Q \propto e^{2\gamma t}$ for $t < t_E$, indicating the quantum-classical correspondence. For $t > t_E$, the OTOCs exhibits a crossover to the power-law increase $C_Q \propto t^{3.3}$, which is different to the quadratic growth of the Hermitian case [73,74]. Note that the exponent 3.3 is independent of λ as long as $\lambda \geqslant 0.007$. The crossover might be due to the onset of quantum interference effects resulting in the dynamical localization. In addition, the C_Q increases with the increase of λ during the time interval $t < t_E$, which demonstrates the enhancement of scrambling by non-Hermitian driven term. As a further step, we numerically investigate both the growth rate γ of C_Q and classical Lyapunov exponent γ_{LE} of the Hermitian kicked rotor model for different K. Analytical prediction of γ_{LE} takes the form $\gamma_{LE} \approx 2\ln(K)$ for $K \gg 1$. The comparison of γ with γ_{LE} demonstrates that the γ for very small λ is larger than the $\gamma_{LE} \approx \ln(K/2)$ roughly in the order of $\ln\sqrt{2}$ [see Fig. 5(b)], which is consistent with the results in Ref. [73]. It is worth noting that the γ increases with increasing λ. Therefore, in the semiclassical limit (i.e., $\hbar_{\text{eff}} \to 0$), the dynamics of OTOCs of our model is qualitatively the same as that of the Hermitian kicked rotor model for $t < t_E$. The influence of quantum effects in non-Hermitian case is characterized by the power-law growth of C_Q with an exponent ≈ 3.3 for a long-term evolution.

V. CONCLUSION AND DISCUSSIONS

One effective strategy for modulating quantum dynamics involves implementing Floquet driven potentials in systems, which has been accomplished by state-of-the-art experiments in both atom optics and optical waveguides. In this paper, we investigate the interesting problems of the phase modulation of the directed transport, time dependence of the energy, and quantum scrambling, in a NQKR model with quantum resonance condition. We uncover a dynamical crossover in time-dependent behaviors of these phenomena. For short time interval $t \ll t_c$, the $\langle p\rangle$, $\langle p^2\rangle$, and C all exhibit quadratic

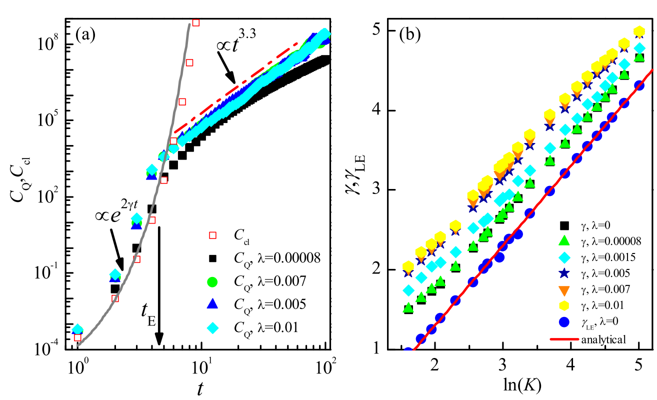

FIG. 5. (a) The C_{cl} (empty squares) and C_Q vs time for $\lambda = 0.00008$ (squares), 0.007 (circles), 0.005 (triangles), and 0.01 (diamonds). Solid line and dash-dotted line indicate the fitting function of the form $C \propto e^{2\gamma t}$ and $C \propto t^{3.3}$, respectively. Arrow marks the Ehrenfest time t_E. The parameters are $K = 8$ and $\hbar_{\text{eff}} = 0.003$. (b) The γ and γ_{LE} (circles) vs $\ln(K)$. The γ_{LE} is evaluated for $\lambda = 0$. The values of non-Hermitian parameter are $\lambda = 0$ (squares), 0.00008 (up triangles), 0.0015 (diamonds), 0.005 (pentagrams), 0.007 (down triangles), and 0.01 (hexagons). Red-solid line indicates the relation $\gamma_{LE} = 2\ln(K)$.

growth with time, and their growth rates depend on λ. After sufficiently long time evolution $t \gg t_c$, the $\langle p \rangle$ shows a linear growth independent of λ, the $\langle p^2 \rangle$ transitions to the λ-independent quadratic growth with time, and the C exhibits a linear growth dependent on the λ. These exotic behaviors are in perfect agreement with our analytical predictions. Based on the second derivative, namely, S_p, S_E, and S_C of these observables, we obtain the phase diagram of the crossover in the parameter space (t, λ), which clearly presents three distinct zones for the dynamics of the momentum current, quantum diffusion, and quantum scrambling. For the quantum nonresonance case, i.e., $\hbar_{\text{eff}} = 4\pi + \Delta$, the $\langle p \rangle$, $\langle p^2 \rangle$, and C exhibit saturation with time evolution, with the saturation levels being adjusted by ϕ. In the semiclassical limit, i.e., $\hbar_{\text{eff}} \to 0$, the C_Q increases exponentially with time, and its growth rate exceeds the classical Lyapunov exponent by a constant factor.

The kicked rotor model and its variants are paradigmatic systems in different fields of physics [77,78], involving interesting topics such as quantum-classical transition [79,80], dynamical phase transition [22], many-body dynamics [54,55,81], and topologically new phases [57–59]. Our study will attract interest in the community of people working in driven systems, such as applying the mapping in Ref. [82] to see if dynamical localization in the non-Hermitian kicked rotor might be connected to localization in a non-Hermitian Anderson model.

Our system in Eq. (1) is achievable in the state-of-the-art atom-optics experiments. Both the expectation values, such as $\langle p \rangle$ and $\langle p^2 \rangle$, and the variance can be detected via time-of-flight measurement of the probability density in momentum space [16,22], paving the way for the experimental validation of our findings. On other aspect, the all-optical systems also serve as ideal platform to realize our non-Hermitian Floquet model, owing to the equivalence between the light propagation equation under paraxial approximation and the Schrödinger equation [83,84]. In Ref. [70], the author has proposed an optical setup involving a Fabry-Perot resonator with flat end mirrors and intracavity phase and loss gratings to emulate the quantum dynamics of the non-Hermitian kicked rotor model. In this system, the reflection of light by the mirrors simulates delta kicking, with the distance between the intracavity mirrors controlling the value of the effective Planck constant. The phase of the loss gratings can be precisely adjusted by etching the surface to different depths [85], which ensures the implementation of kicking potentials with all kinds of symmetries. The mean value of observables can be measured in the frequency domain of optics, enabling the observation of our findings.

ACKNOWLEDGMENTS

We thank Dr. Shen for valuable discussion on the possibility of experimental realization of in optical systems. W.-L.Z. is supported by the National Natural Science Foundation of China (Grants No. 12065009 and No. 12365002), the Natural Science Foundation of Jiangxi province (Grants No. 20224ACB201006 and No. 20224BAB201023) and the Science and Technology Planning Project of Ganzhou City (Grant No. 202101095077). J.L. is supported by the NSAF (Contract No. U2330401).

APPENDIX: PROPERTIES OF THE MODIFIED BESSEL FUNCTIONS OF THE FIRST KIND

The modified Bessel functions of the first kind are defined by

$$I_m(x) = \frac{1}{2\pi} \int_0^{2\pi} e^{-im\theta} \exp\left[x \cos(\theta)\right] d\theta. \tag{A1}$$

The function $I_m(x)$ can be expanded as

$$I_m(x) = \frac{e^x}{\sqrt{2\pi x}}\Bigg[1 - \frac{4m^2-1}{8x} + \frac{(4m^2-1)(4m^2-9)}{2!(8x)^2} - \frac{(4m^2-1)(4m^2-9)(4m^2-25)}{3!(8x)^3} + \cdots\Bigg]. \tag{A2}$$

Our theoretical analysis involves the function $I_m(x)$ with $0 \leqslant m \leqslant 3$. For $x \ll 1$, they can be approximated as

$$I_0(x) \approx 1, \quad I_1(x) \approx \frac{x}{2}, \quad I_2(x) \approx \frac{x^2}{8}, \quad \text{and } I_3(x) \approx \frac{x^3}{48}. \tag{A3}$$

For $x \gg 1$, the two leading terms in Eq. (A2) contribute significantly. Therefore, we have neglected the other terms and obtained the following relations:

$$I_0(x) \approx \frac{e^x}{\sqrt{2\pi x}}\left(1 + \frac{1}{8x}\right), \tag{A4}$$

$$I_1(x) \approx \frac{e^x}{\sqrt{2\pi x}}\left(1 - \frac{3}{8x}\right), \tag{A5}$$

$$I_2(x) \approx \frac{e^x}{\sqrt{2\pi x}}\left(1 - \frac{15}{8x}\right), \tag{A6}$$

and

$$I_3(x) \approx \frac{e^x}{\sqrt{2\pi x}}\left(1 - \frac{35}{8x}\right). \tag{A7}$$

[1] A. Kenfack, J. B. Gong, and A. K. Pattanayak, Controlling the ratchet effect for cold atoms, Phys. Rev. Lett. **100**, 044104 (2008).

[2] C. Hainaut, A. Rançon, J. F. Clément, J. C. Garreau, P. Szriftgiser, R. Chicireanu, and D. Delande, Ratchet effect in the quantum kicked rotor and its destruction by dynamical localization, Phys. Rev. A **97**, 061601(R) (2018).

[3] Z. Q. Li, X. X. Hu, J. P. Xiao, Y. J. Chen, and X. B. Luo, Ratchet current in a $\mathcal{PT}$-symmetric Floquet quantum system with symmetric sinusoidal driving, Phys. Rev. A **108**, 052211 (2023).

[4] D. Poletti, G. Benenti, G. Casati, and B. W. Li, Interaction-induced quantum ratchet in a Bose-Einstein condensate, Phys. Rev. A **76**, 023421 (2007).

[5] J. B. Gong and P. Brumer, Coherent control of quantum chaotic diffusion, Phys. Rev. Lett. **86**, 1741 (2001).

[6] M. Bitter and V. Milner, Experimental demonstration of coherent control in quantum chaotic systems, Phys. Rev. Lett. **118**, 034101 (2017).

[7] M. A. Sentef, J. J. Li, F. Künzel, and M. Eckstein, Quantum to classical crossover of Floquet engineering in correlated quantum systems, Phys. Rev. Res. **2**, 033033 (2020).

[8] S. Y. Bai and J. H. An, Floquet engineering to reactivate a dissipative quantum battery, Phys. Rev. A **102**, 060201(R) (2020).

[9] C. A. Downing and M. S. Ukhtary, A quantum battery with quadratic driving, Commun. Phys. **6**, 322 (2023).

[10] E. J. Meier, J. Ang'ong'a, F. A. An, and B. Gadway, Exploring quantum signatures of chaos on a Floquet synthetic lattice, Phys. Rev. A **100**, 013623 (2019).

[11] J. H. Wang, T.-Q. Cai, X.-Y. Han, Y.-W Ma, Z.-L Wang, Z.-H Bao, Y. Li, H.-Y Wang, H.-Y Zhang, L.-Y Sun, Y.-K. Wu, Y.-P. Song, and L.-M. Duan, Information scrambling dynamics in a fully controllable quantum simulator, Phys. Rev. Res. **4**, 043141 (2022).

[12] J. Harris, B. Yan, and N. A. Sinitsyn, Benchmarking information scrambling, Phys. Rev. Lett. **129**, 050602 (2022).

[13] Q. Q. Cheng, Y. M. Pan, H. Q. Wang, C. S. Zhang, D. Yu, A. Gover, H. J. Zhang, T. Li, L. Zhou, and S. N. Zhu, Observation of anomalous π modes in photonic Floquet engineering, Phys. Rev. Lett. **122**, 173901 (2019).

[14] X. G. Wang, L. L. Zeng, G. H. Guo, and J. Berakdar, Floquet engineering the exceptional points in parity-time-symmetric magnonics, Phys. Rev. Lett. **131**, 186705 (2023).

[15] J. B. Gong and P. Brumer, Phase control of nonadiabaticity-induced quantum chaos in an optical lattice, Phys. Rev. Lett. **88**, 203001 (2002).

[16] C. Hainaut, I. Manai, J.-F. Clément, J. C. Garreau, P. Szriftgiser, G. Lemarié, N. Cherroret, D. Delande, and R. Chicireanu, Controlling symmetry and localization with an artificial gauge field in a disordered quantum system, Nat. Commun. **9**, 1382 (2018).

[17] C. Tian and A. Altland, Theory of localization and resonance phenomena in the quantum kicked rotor, New J. Phys. **12**, 043043 (2010).

[18] J. C. Garreau and V. Zehnlé, Analog quantum simulation of the spinor-four Dirac equation with an artificial gauge field, Phys. Rev. A **101**, 053608 (2020).

[19] G. Casati, I. Guarneri, and D. L. Shepelyansky, Anderson transition in a one-dimensional system with three incommensurate frequencies, Phys. Rev. Lett. **62**, 345 (1989).

[20] D. L. Shepelyansky, Localization of diffusive excitation in multi-level systems, Physica D **28**, 103 (1987).

[21] C. S. Tian, A. Altland, and M. Garst, Theory of the Anderson transition in the quasiperiodic kicked rotor, Phys. Rev. Lett. **107**, 074101 (2011).

[22] C. Hainaut, P. Fang, A. Rançon, J. F. Clément, Pascal Szriftgiser, J. C Garreau, C. S. Tian, and R. Chicireanu, Experimental observation of a time-driven phase transition in quantum chaos, Phys. Rev. Lett. **121**, 134101 (2018).

[23] M. Lopez, J. F. Clément, P. Szriftgiser, J. C. Garreau, and D. Delande, Experimental test of universality of the Anderson transition, Phys. Rev. Lett. **108**, 095701 (2012).

[24] M. Lopez, J. F. Clément, G. Lemarié, D. Delande, P. Szriftgiser and J. C. Garreau, Phase diagram of the anisotropic Anderson transition with the atomic kicked rotor: Theory and experiment, New J. Phys. **15**, 065013 (2013).

[25] I. Manai, J.-F. Clément, R. Chicireanu, C. Hainaut, J. C. Garreau, P. Szriftgiser, and D. Delande, Experimental observation of two-dimensional Anderson localization with the atomic kicked rotor, Phys. Rev. Lett. **115**, 240603 (2015).

[26] D. O. Chudesnikov and V. P. Yakovlev, Bragg scattering on complex potential and formation of super-narrow momentum distributions of atoms in light fields, Laser Phys. **1**, 110 (1991).

[27] C. Keller, M. K. Oberthaler, R. Abfalterer, S. Bernet, J. Schmiedmayer, and A. Zeilinger, Tailored complex potentials and Friedel's law in atom optics, Phys. Rev. Lett. **79**, 3327 (1997).

[28] C. M. Bender and S. Boettcher, Real spectra in non-Hermitian Hamiltonians having PT symmetry, Phys. Rev. Lett. **80**, 5243 (1998).

[29] J. B. Gong and Q. H. Wang, Time-dependent $\mathcal{PT}$-symmetric quantum mechanics, J. Phys. A **46**, 485302 (2013).

[30] C. Wang, W. R. Sweeney, A. D. Stone, and L. Yang, Coherent perfect absorption at an exceptional point, Science **373**, 1261 (2021).

[31] Ş. K. Özdemir, S. Rotter, F. Nori, and L. Yang, Parity-time symmetry and exceptional points in photonics, Nat. Mater. **18**, 783 (2019).

[32] Y. Song, W. Liu, L. Zheng, Y. Zhang, B. Wang, and P. Lu, Two-dimensional non-Hermitian skin effect in a synthetic photonic lattice, Phys. Rev. Appl. **14**, 064076 (2020).

[33] H. C. Li, C. Luo, T. L. Zhang, X. Zhou, J. W. Xu, J. W. Xu, S. X. Duan, X. H. Deng, and Y. Shen, Non-Hermitian total-loss high-order topological insulator based on 1D Su-Schrieffer-Heeger (SSH), Phys. B: Condens. Matter, **650**, 414570 (2023).

[34] Y. Shen, J. Ji, H.-C. Li, L. Zhang, X. Yu, S.-B. Yan, M. Rasmussen, Q. Shen, D. Madhi, B.-B. Zhou, P. U. Jepsen, and X.-H. Deng, Realization of photonic topological insulators at terahertz frequencies characterized by time-domain spectroscopy, Phys. Rev. Appl. **18**, 064025 (2022).

[35] H. C. Li, C. Luo, T. L. Zhang, J. W. Xu, X. Zhou, Y. Shen, and X. H. Deng, Topological refraction in kagome split-ring photonic insulators, Nanomaterials **12**, 1493 (2022).

[36] L. Zhang, Y. Yang, Y. Ge, Y.-J. Guan, Q. Chen, Q. Yan, F. Chen, R. Xi, Y. Li, D. Jia, S.-Q. Yuan *et al.*, Acoustic non-Hermitian skin effect from twisted winding topology, Nat. Commun. **12**, 6297 (2021).

[37] X. F. Zhu, H. Ramezani, C. Z. Shi, J. Zhu, and X. Zhang, $\mathcal{PT}$-symmetric acoustics, Phys. Rev. X **4**, 031042 (2014).

[38] H. X. Zhang, T. Chen, L. H. Li, C. H. Lee, and X. D. Zhang, Electrical circuit realization of topological switching for the non-Hermitian skin effect, Phys. Rev. B **107**, 085426 (2023).

[39] M. Chitsazi, H. N. Li, F. M. Ellis, and T. Kottos, Experimental realization of Floquet $\mathcal{PT}$-symmetric systems, Phys. Rev. Lett. **119**, 093901 (2017).

[40] K. Sim, N. Defenu, P. Molignini, and R. Chitra, Quantum metric unveils defect freezing in non-Hermitian systems, Phys. Rev. Lett. **131**, 156501 (2023).

[41] W. Y. Wang, B. Sun, and J. Liu, Adiabaticity in nonreciprocal Landau-Zener tunneling, Phys. Rev. A **106**, 063708 (2022).

[42] X. Tong, X. Gao, and S.-P. Kou, Adiabatic-impulse approximation in the non-Hermitian Landau-Zener model, Phys. Rev. B **107**, 104306 (2023).

[43] X. Wang, H. D. Liu, and L. B. Fu, Nonlinear non-Hermitian Landau-Zener-Stückelberg-Majorana interferometry, New J. Phys. **25**, 043032 (2023).

[44] W. L. Zhao, J. Z. Wang, X. H. Wang, and P. Q. Tong, Directed momentum current induced by the $\mathcal{PT}$-symmetric driving, Phys. Rev. E **99**, 042201 (2019).

[45] W. L. Zhao, Quantization of out-of-time-ordered correlators in non-Hermitian chaotic systems, Phys. Rev. Res. **4**, 023004 (2022).

[46] W. L. Zhao, R. R. Wang, H. Ke, and J. Liu, Scaling laws of the out-of-time-order correlators at the transition to the spontaneous $\mathcal{PT}$-symmetry breaking in a Floquet system, Phys. Rev. A **107**, 062201 (2023).

[47] K. Yokomizo and S. Murakami, Non-Bloch band theory of non-Hermitian systems, Phys. Rev. Lett. **123**, 066404 (2019).

[48] F. Song, S. Yao, and Z. Wang, Non-Hermitian skin effect and chiral damping in open quantum systems, Phys. Rev. Lett. **123**, 170401 (2019).

[49] L. W. Zhou and D.-J. Zhang, Non-Hermitian Floquet topological matter—A review, Entropy **25**, 1401 (2023).

[50] S. Z. Li, X. J. Yu, and Z. Li, Emergent entanglement phase transitions in non-Hermitian Aubry-André-Harper chains, Phys. Rev. B **109**, 024306 (2024).

[51] H. Y. Meng, Y. S. Ang, and C. H. Lee, Exceptional points in non-Hermitian photonics: Applications and recent developments, arXiv:2310.16699.

[52] H. Cao and J. Wiersig, Dielectric microcavities: Model systems for wave chaos and non-Hermitian physics, Rev. Mod. Phys. **87**, 61 (2015).

[53] B. Toloui and L. E. Ballentine, Quantum localization for two coupled kicked rotors, arXiv:0903.4632.

[54] S. Notarnicola, F. Iemini, D. Rossini, R. Fazio, A. Silva, and A. Russomanno, From localization to anomalous diffusion in the dynamics of coupled kicked rotors, Phys. Rev. E **97**, 022202 (2018).

[55] A. Russomanno, M. Fava, and R. Fazio, Chaos and subdiffusion in infinite-range coupled quantum kicked rotors, Phys. Rev. B **103**, 224301 (2021).

[56] S. Dadras, A. Gresch, C. Groiseau, S. Wimberger, and G. S. Summy, Experimental realization of a momentum-space quantum walk, Phys. Rev. A **99**, 043617 (2019).

[57] D. Y. H. Ho and J. B. Gong, Quantized adiabatic transport in momentum space, Phys. Rev. Lett. **109**, 010601 (2012).

[58] L. W. Zhou and J. X. Pan, Non-Hermitian Floquet topological phases in the double-kicked rotor, Phys. Rev. A **100**, 053608 (2019).

[59] Y. Chen and C. S. Tian, Planck's quantum-driven integer quantum Hall effect in chaos, Phys. Rev. Lett. **113**, 216802 (2014).

[60] Z. Qi, T. Scaffidi, and X. Cao, Surprises in the deep Hilbert space of all-to-all systems: From superexponential scrambling to slow entanglement growth, Phys. Rev. B **108**, 054301 (2023).

[61] X. D. Hu, T. Luo, and D. B. Zhang, Quantum algorithm for evaluating operator size with Bell measurements, Phys. Rev. A **107**, 022407 (2023).

[62] J. Wang, G. Benenti, G. Casati, and W. G. Wang, Quantum chaos and the correspondence principle, Phys. Rev. E **103**, L030201 (2021).

[63] S. Pappalardi and J. Kurchan, Low temperature quantum bounds on simple models, SciPost Phys. **13**, 006 (2022).

[64] R. J. Lewis-Swan, A. Safavi-Naini, J. J. Bollinger, and A. M. Rey, Unifying scrambling, thermalization and entanglement through measurement of fidelity out-of-time-order correlators in the Dicke model, Nat. Commun. **10**, 1581 (2019).

[65] In current studies of non-Hermitian systems, the re-normalization is a standard and conventional method for dealing with the changing norm. In a recent paper [40], a different dynamical metric is proposed, in which both left vector and right vector are involved to deal with the changing norm.

[66] W. L. Zhao and J. Liu, Quantum criticality at the boundary of the non-Hermitian regime of a Floquet system, Phys. Rev. A **109**, 052215 (2024).

[67] J. T. Edwards and D. J. Thouless, Numerical studies of localization in disordered systems, J. Phys. C: Solid State Phys. **5**, 807 (1972).

[68] B. Lévi, B. Georgeot, and D. L. Shepelyansky, Quantum computing of quantum chaos in the kicked rotator model, Phys. Rev. E **67**, 046220 (2003).

[69] Q. Wang and M. Robnik, Statistics of phase space localization measures and quantum chaos in the kicked top model, Phys. Rev. E **107**, 054213 (2023).

[70] S. Longhi, Localization, quantum resonances, and ratchet acceleration in a periodically kicked $\mathcal{PT}$-symmetric quantum rotator, Phys. Rev. A **95**, 012125 (2017).

[71] B. V. Chirikov, in *Chaos and Quantum Mechanics*, Les Houches Lecture Series Vol. 52 edited by M.-J. Giannoni, A. Voros, and J. Zinn-Justin (Elsevier Science, Amsterdam, 1991), pp. 443-545.

[72] The saturated values of the momentum current, mean energy, and OTOCs can be quantified by their time-averaged values, i.e., $\overline{\langle p\rangle} = \sum_{j=1}^{N}\langle p(t_j)\rangle/N$, $\overline{\langle p^2\rangle} = \sum_{j=1}^{N}\langle p^2(t_j)\rangle/N$, and $\overline{C} = \sum_{j=1}^{N} C(t_j)/N$, where N is the total number of kicking times. In numerical simulations, we find that for relatively large Δ (e.g., $\Delta = 0.1$), using one thousand kick periods $N = 1000$ can ensure the good approximation of the saturated values by $\overline{\langle p\rangle}$, $\overline{\langle p^2\rangle}$, and $\overline{C}$.

[73] E. B. Rozenbaum, S. Ganeshan, and V. Galitski, Lyapunov exponent and out-of-time-ordered correlator's growth rate in a chaotic system, Phys. Rev. Lett. **118**, 086801(R) (2017).

[74] R. Hamazaki, K. Fujimoto, and M. Ueda, Operator noncommutativity and irreversibility in quantum chaos, arXiv:1807.02360.

[75] E. M. Graefe, M. Hoening, and H. J. Korsch, Classical limit of non-Hermitian quantum dynamics—A generalized canonical structure, J. Phys. A: Math. Theor. **43**, 075306 (2010).

[76] Z. Zou and J. Wang, A pseudoclassical theory for the wavepacket dynamics of the kicked rotor model, Sci. China Phys. Mech. Astron., **67**, 230511 (2024).

[77] F. M. Izrailev, Simple models of quantum chaos: Spectrum and eigenfunctions, Phys. Rep. **196**, 299 (1990).

[78] M. S. Santhanam, S. Paul, and J. B. Kannan, Quantum kicked rotor and its variants: Chaos, localization and beyond, Phys. Rep. **956**, 1 (2022).

[79] S. Adachi, M. Toda, and K. Ikeda, Potential for mixing in quantum chaos, Phys. Rev. Lett. **61**, 655 (1988).

[80] D. Cohen, Quantum chaos, dynamical correlations, and the effect of noise on localization, Phys. Rev. A **44**, 2292 (1991).

[81] A. Russomanno, Spatiotemporally ordered patterns in a chain of coupled dissipative kicked rotors, Phys. Rev. B **108**, 094305 (2023).

[82] S. Fishman, D. R. Grempel, and R. E. Prange, Chaos, quantum recurrences, and anderson localization, Phys. Rev. Lett. **49**, 509 (1982).

[83] B. Fischer, A. Rosen, A. Bekker, and S. Fishman, Experimental observation of localization in the spatial frequency domain of a kicked optical system, Phys. Rev. E **61**, R4694(R) (2000).

[84] A. Rosen, B. Fischer, A. Bekker, and S. Fishman, Optical kicked system exhibiting localization in the spatial frequency domain, J. Opt. Soc. Am. B **17**, 1579 (2000).

[85] C. Zhang, C. F. Li, and G. C. Guo, Experimental demonstration of photonic quantum ratchet, Sci. Bull. **60**, 249 (2015).